MIT Libraries | DSpace@MIT

MIT Open Access Articles

Modulation of Monsoon Circulations by Cross-Equatorial Ocean Heat Transport

The MIT Faculty has made this article openly available. ***Please share*** how this access benefits you. Your story matters.

Citation: Lutsko, Nicholas J. et. al., "Modulation of Monsoon Circulations by Cross-Equatorial Ocean Heat Transport." Journal of Climate 32, 12 (May 2019): 3471-85 doi. 10.1175/JCLI-D-18-0623.1 ©2019 Authors

As Published: 10.1175/JCLI-D-18-0623.1

Publisher: American Meteorological Society

Persistent URL: https://hdl.handle.net/1721.1/124955

Version: Final published version: final published article, as it appeared in a journal, conference proceedings, or other formally published context

Terms of Use: Article is made available in accordance with the publisher's policy and may be subject to US copyright law. Please refer to the publisher's site for terms of use.

Massachusetts Institute of Technology

Modulation of Monsoon Circulations by Cross-Equatorial Ocean Heat Transport

NICHOLAS J. LUTSKO AND JOHN MARSHALL

Department of Earth, Atmospheric, and Planetary Sciences, Massachusetts Institute of Technology, Cambridge, Massachusetts

BRIAN GREEN

Joint Institute for the Study of the Atmosphere and Ocean, University of Washington, Seattle, Washington

(Manuscript received 20 September 2018, in final form 4 March 2019)

ABSTRACT

Motivated by observations of southward ocean heat transport (OHT) in the northern Indian Ocean during summer, the role of the ocean in modulating monsoon circulations is explored by coupling an atmospheric model to a slab ocean with an interactive representation of OHT and an idealized subtropical continent. Southward OHT by the cross-equatorial cells is caused by Ekman flow driven by southwesterly monsoon winds in the summer months, cooling sea surface temperatures (SSTs) south of the continent. This increases the reversed meridional surface gradient of moist static energy, shifting the precipitation maximum over the land and strengthening the monsoonal circulation, in the sense of enhancing the vertical wind shear. However, the atmosphere's cross-equatorial meridional overturning circulation is also weakened by the presence of southward OHT, as the atmosphere is required to transport less energy across the equator. The sensitivity of these effects to varying the strength of the OHT, fixing the OHT at its annual-mean value, and to removing the land is explored. Comparisons with more realistic models suggest that the idealized model used in this study produces a reasonable representation of the effect of OHT on SSTs equatorward of subtropical continents, and hence can be used to study the role of OHT in shaping monsoon circulations on Earth.

1. Introduction

It is now well understood that the South Asian monsoon is a thermally direct circulation, driven by the thermodynamic contrast that develops in the summer months between the Indian subcontinent and the Indian Ocean to the south (e.g., Plumb and Hou 1992; Privé and Plumb 2007a,b; Bordoni and Schneider 2008; Zhai and Boos 2015; Geen et al. 2018). Intuitively, this contrast arises because the land's smaller heat capacity causes it to warm up faster in the summer than the surrounding waters, but recent work has shown that a number of other factors are required to maintain the gradient. Most importantly, the Himalayas play a crucial role by insulating the Indian subcontinent from cold northerly winds blowing down from central Eurasia, keeping surface temperatures over India high during summer [see Boos and Kuang (2010) and Ma et al. (2014)].

The other side of the contrast—the relatively cool waters of the northern Indian Ocean (NIO)—has been less explored. Privé and Plumb (2007b) compared the monsoons in simulations with their idealized atmospheric model forced by uniformly warm sea surface temperatures (SSTs) and by an SST profile that has a meridional gradient, and found that a meridional SST gradient promotes a cross-equatorial monsoon circulation. This picture was complicated, however, because the land in their idealized setup is cooled by zonal winds coming from the colder waters adjacent to the land, damping the thermal contrast and hence the monsoon circulation (see also Chou et al. 2001). Privé and Plumb were able to strengthen the monsoon in their model by adding "walls" around the continent to insulate it from these sea breezes.

While this provided a first indication of the relationship between the NIO and the monsoon circulation, it was highly idealized and did not consider feedbacks between the monsoonal winds and the SSTs. Webster

Denotes content that is immediately available upon publication as open access.

Corresponding author: Nicholas Lutsko, lutsko@mit.edu

DOI: 10.1175/JCLI-D-18-0623.1

© 2019 American Meteorological Society. For information regarding reuse of this content and general copyright information, consult the AMS Copyright Policy (www.ametsoc.org/PUBSReuseLicenses).

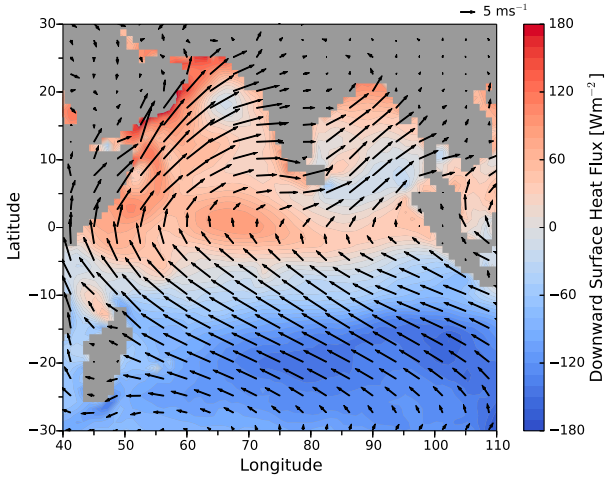

FIG. 1. Climatological June–August (JJA) downward energy flux at the ocean surface (contours) and surface winds (arrows) from the NCEP reanalysis for the period 1979–2011.

and coauthors have suggested that the monsoon acts as a self-regulating system (Loschnigg and Webster 2000; Webster et al. 2002; Chirokova and Webster 2006), with strong monsoonal winds driving southward ocean heat transport (OHT) in the NIO, cooling the waters adjacent to the Indian subcontinent and hence damping the monsoon. This can be seen in observations, as the surface winds are southwesterly over the NIO in the summer and southeasterly south of the equator (arrows in Fig. 1). This circulation pattern drives southward Ekman flow in the NIO's mixed layer, transporting heat into the Southern Hemisphere and potentially cooling the SSTs of the NIO. The heat transport can be inferred from the contours in Fig. 1, which show the flux of heat from the atmosphere into the ocean. Developing a better understanding of the connection between OHT and monsoon circulations is the primary aim of this study.

The role of the Indian Ocean in cross-equatorial heat transport has been appreciated as far back as at least Levitus (1987) (see also Lee and Marotzke 1998). Levitus hypothesized that the Ekman response to near surface equatorial winds in the Indian Ocean results in southward cross-equatorial heat transport in the boreal summer, which reverses in winter. Ideas that describe the dynamical process involved (those of the cross-equatorial cell) are developed in McCreary et al. (1993), whose model was adapted by Loschnigg and Webster (2000) and Chirokova and Webster (2006).

Separate from the question of monsoons, the relationship between the zonal-mean atmospheric circulation and OHT has been investigated in a number of recent studies. It has been shown that including interactive OHT in idealized models substantially damps the Hadley circulation (Clement 2006; Levine and Schneider 2011; Singh et al. 2017; Hilgenbrink and Hartmann 2018), as well as meridional shifts of the intertropical convergence zone [ITCZ; Green and Marshall 2017; Schneider 2017; however, note that Clement (2006) found that OHT increases the amplitude of the seasonal migration of the ITCZ]. The reason for this is that, because of its small gross moist stability, the tropical atmosphere is an inefficient transporter of energy (Held 2001). By contrast, the wind-driven subtropical cells in the ocean efficiently transport energy away from the equator because of the large surface temperature difference between the tropics and subtropics, which is mapped onto the vertical via subduction (Klinger and Marotzke 2000; Held 2001; Czaja and Marshall 2006; Green and Marshall 2017). Hence including interactive OHT means that much less energy needs to be transported to high latitudes by the atmosphere. These studies have focused on the zonal-mean perspective, but similar considerations would be expected to apply to zonally asymmetric perturbations, such as monsoons, with the caveat that we do not yet have a good understanding of what controls the partitioning between zonal and meridional energy transports.

Putting these results together, coupling to the ocean has a number of competing effects on monsoonal circulations, potentially strengthening them by enhancing land–sea temperature gradients and potentially weakening them by cooling the waters adjacent to landmasses and by reducing the energetic requirements on the cross-equatorial atmospheric circulation. Motivated by the geographic setting of the South Asian monsoon, in this study we take a first step toward untangling the effects of ocean dynamics on monsoon circulations by investigating how the monsoon in a moist, gray radiation atmospheric general circulation model (GCM) is affected by coupling the GCM to a slab ocean with an interactive representation of OHT. The parameterization includes an ocean stratification parameter that can be varied to directly control the strength of the OHT, allowing us to systematically investigate the influence of OHT on the monsoon. We have also performed sensitivity experiments without land and with the OHT fixed at its annual-mean value to separate zonally asymmetric effects from zonal-mean effects and to cut the coupling between OHT and the monsoonal circulation.

We note that our focus is primarily on the seasonal-mean monsoon and not on monsoonal variability. Work with observations and with comprehensive models has demonstrated a strong link between monsoon variability and SSTs; for instance, colder SSTs in the Bay of Bengal precede "breaks" in the South Asian monsoon, periods when the rains are muted, by about a week (e.g., Vecchi

and Harrison 2002; Schott et al. 2009). However, this kind of variability is unlikely to be well represented in our model, and our focus is instead on the seasonal-mean state of the monsoon, which the model can be expected to represent, at least in an idealized sense, and on the more general question of the relationship between zonally asymmetric atmospheric circulations and OHT.

The model and the simulations we have performed are described in more detail in the next section. In section 3 we investigate how the monsoon in our model is affected by coupling with the OHT parameterization, including how it is affected by varying the strength of the OHT and by fixing the OHT at its annual-mean value. In section 4 we compare the model with more realistic coupled models to assess how relevant our results may be for the South Asian monsoon and in section 5 we present the results of experiments without land. We end with conclusions in section 6.

2. Model description and simulations

The model consists of the idealized moist GCM first described by Frierson et al. (2006), coupled to a slab ocean with an idealized representation of OHT by the subtropical cells.

a. The moist GCM

The GCM solves the primitive equations on the sphere and uses gray radiative transfer. The longwave optical depth τ is specified to approximate the effects of atmospheric water vapor (Frierson et al. 2006):

$$\tau(p,\phi) = \tau_0\left[f_l\left(\frac{p}{p_s}\right) + (1-f_l)\left(\frac{p}{p_s}\right)^4\right], \tag{1}$$

where p is pressure, ϕ is latitude, p_s is the surface pressure and the linear term is included to reduce stratospheric relaxation times (f_1 is set to 0.1). Here, τ_0 is the optical depth at the surface, and takes the form

$$\tau_0(\phi) = \tau_{0e} + (\tau_{0p} - \tau_{0e})\sin^2\phi, \tag{2}$$

with τ_{0e} being the surface value at the equator and τ_{0p} the surface value at the pole. These are set to 7.2 and 1.8, respectively, following O'Gorman and Schneider (2008). The solar insolation has an annual cycle, but no diurnal cycle, and is calculated as [see chapter 2 of Hartmann (2016)]

$$S_0 = \frac{S_c}{\pi}(h_0\sin\phi\sin\delta + \cos\phi\cos\delta\sin h_0), \tag{3}$$

where the solar constant S_c is set to 1360 W m^{-2}; h_0 is the longitude of the subsolar point at sunrise and sunset relative to its position at noon; and δ is the declination, calculated using an obliquity of 23.45° and a 360-day year and assuming that Earth's orbit is perfectly circular. The albedo is fixed at 0.38 and absorption of solar radiation by the atmosphere is modeled by calculating the downward shortwave flux at a given pressure level as $S = S_0\exp[-\tau_s(p/p_s)^2]$, with τ_s fixed at 0.22, also following O'Gorman and Schneider (2008).

The model includes the simplified Betts–Miller (SBM) convection scheme of Frierson (2007), with a convective relaxation time scale τ_{SBM} of 2 h and a reference relative humidity $\mathrm{RH}_{\mathrm{SBM}} = 0.7$, and the boundary layer scheme is the one used by O'Gorman and Schneider (2008). In each experiment the model was integrated for 8 years at T85 truncation (corresponding to a resolution of roughly 1.4° × 1.4° on a Gaussian grid) with 30 vertical levels extending up to 16 hPa. Averages were taken over the last 7 years of each simulation.

b. Interactive OHT parameterization

OHT can be represented as the product of a meridional overturning circulation and an energy contrast (Held 2001; Czaja and Marshall 2006)

$$q_O = c_{p,o}\Phi\Delta T, \tag{4}$$

where $c_{p,o}$ is the heat capacity of seawater, Φ is the overturning mass transport streamfunction, and ΔT is the temperature difference across the upper and lower branches of the overturning circulation (i.e., between the top and base of the subtropical cells). This can also be thought of as the surface temperature difference between the deep tropics and the latitude of subduction, with typical values of 5–10 K (Klinger and Marotzke 2000).

In the tropics, oceanic mass transport is mostly set by Ekman mass transport, allowing us to approximate the OHT as

$$q_O(\phi,\lambda) \approx ac_{p,o}\cos\phi\frac{\tau(\phi,\lambda)}{f(\phi)}\Delta T, \tag{5}$$

where λ is longitude, a is the radius of Earth, τ is the wind stress, and f is the Coriolis parameter. Our interactive OHT parameterization assumes that heat is only transported via Eq. (5), and only calculates the OHT for latitudes between ϕ_1, the latitude at which the surface winds change from westerly to easterly in the Southern Hemisphere, and ϕ_2, the latitude at which the surface winds change from easterly to westerly in the Northern Hemisphere. Here, $c_{p,o}$ is set to 3900 J kg^{-1} K^{-1} and, importantly, ΔT is left as a free parameter to be specified.

This parameterization is similar to the scheme used by Klinger and Marotzke (2000) and Levine and Schneider

(2011), except that their scheme uses surface quantities, so that the OHT is calculated from the surface wind and temperature fields, with no free parameters. Here we specify ΔT directly in order to systematically investigate how the strength of the OHT impacts the monsoon, as larger ΔT values result in more heat being transported southward in the summer.

As in Levine and Schneider (2011), we apply a Gaussian smoothing filter when calculating the divergence of the heat flux to avoid issues with f going to zero at the equator:

$$(\nabla \cdot q_O)' = \int_{\phi_1}^{\phi_2} \frac{1}{a\cos\phi}(\nabla \cdot q_O)P(\phi,\phi')\,d\phi', \qquad (6)$$

where

$$P(\phi,\phi') = \frac{1}{Z}\exp\left[\frac{-(\phi'-\phi)^2}{2s^2}\right], \qquad (7)$$

with Z chosen such that the integral of P from ϕ_1 to ϕ_2 is equal to one and s a half-width, which is set to 7°.

Two drawbacks of this scheme are that the effective stability, ΔT, is the same at all locations and that the depth of the thermocline is fixed. For example, surface temperatures will warm where there is convergent Ekman mass flux, but in a more realistic model this would also cause the thermocline to deepen, with little warming of the surface waters. As such, we compare our results with a simulation which uses the "1.5-layer" parameterization of Ekman heat transport by Codron (2012), although we have excluded diffusive heat transport and again only focus on heat transport in the tropics. In this scheme the temperature of the return flow, T_d is diagnosed from the surface temperature as

$$T_d = \alpha T_s + (1-\alpha)T_0, \qquad (8)$$

where T_s is the surface temperature, T_0 is a reference temperature, here taken to be 273.15 K, and ΔT is now equal to $T_s - T_d$. Also, α varies linearly from 1/3 for purely divergent flow to 1 for purely convergent flow. This results in an effective stability that is large (up to about 15 K) where there is divergence and small (~0 K) where there is convergence. Codron showed that, with these parameter values, the 1.5-layer scheme produces a reasonable representation of the climatology and seasonal cycle of SSTs when coupled to a comprehensive atmospheric GCM.

Another issue with our parameterization, and also that of Codron, is that the upper and lower branches of the circulation respond quickly to changes in wind stress. In the real ocean, the lower branch responds more slowly to changing wind stress, affecting the net heat transport, which is proportional to the difference in the mass transport in the upper and lower branches. This lag is difficult to capture in simple models, and we leave it for future work to see how it affects our results.

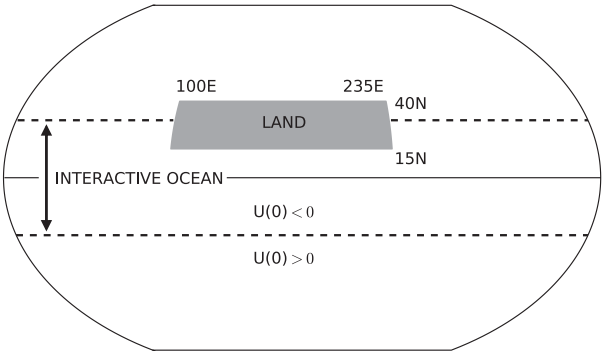

FIG. 2. Schematic of the model configuration used in the experiments. Note that the boundaries of the interactive ocean move seasonally.

The depth of the ocean slab is fixed at 24 m in all simulations. Donohoe et al. (2014) found that coupling the AM2.1 GCM to a 24-m slab ocean produces a climate with a reasonable seasonal migration of the ITCZ compared with observations, and also a reasonable annual-mean Hadley circulation and meridional distribution of precipitation.

"Land" is added to the model by reducing the mixed layer depth to 0.5 m and setting the ocean heat flux divergence to zero within 100°–235°E and 15°–40°N. This provides an infinite supply of moisture for the monsoonal circulation and also means that the global integral of q_O is not always zero. So there may be net OHT from the Northern Hemisphere into the Southern Hemisphere, even for conditions that are otherwise hemispherically symmetric; however, we find that in the annual mean the ITCZ is very close to the equator in all of our simulations (not shown). The geometry of our setup is illustrated in Fig. 2.

c. Simulations

We have performed three sets of simulations with the model, motivated by our aim of untangling the competing effects of OHT on the monsoon. The main set includes both land and the interactive OHT, with ΔT varied from 0 K (i.e., no OHT) to 15 K. In a second set of simulations the OHT at each grid point is fixed at its annual-mean value from the first set of simulations, eliminating the coupling between OHT and the monsoonal circulation but maintaining the annual-mean effects of OHT. The third set includes the interactive OHT but not the land, with ΔT again varied from 0 to 15 K. Comparing these simulations with the first set of

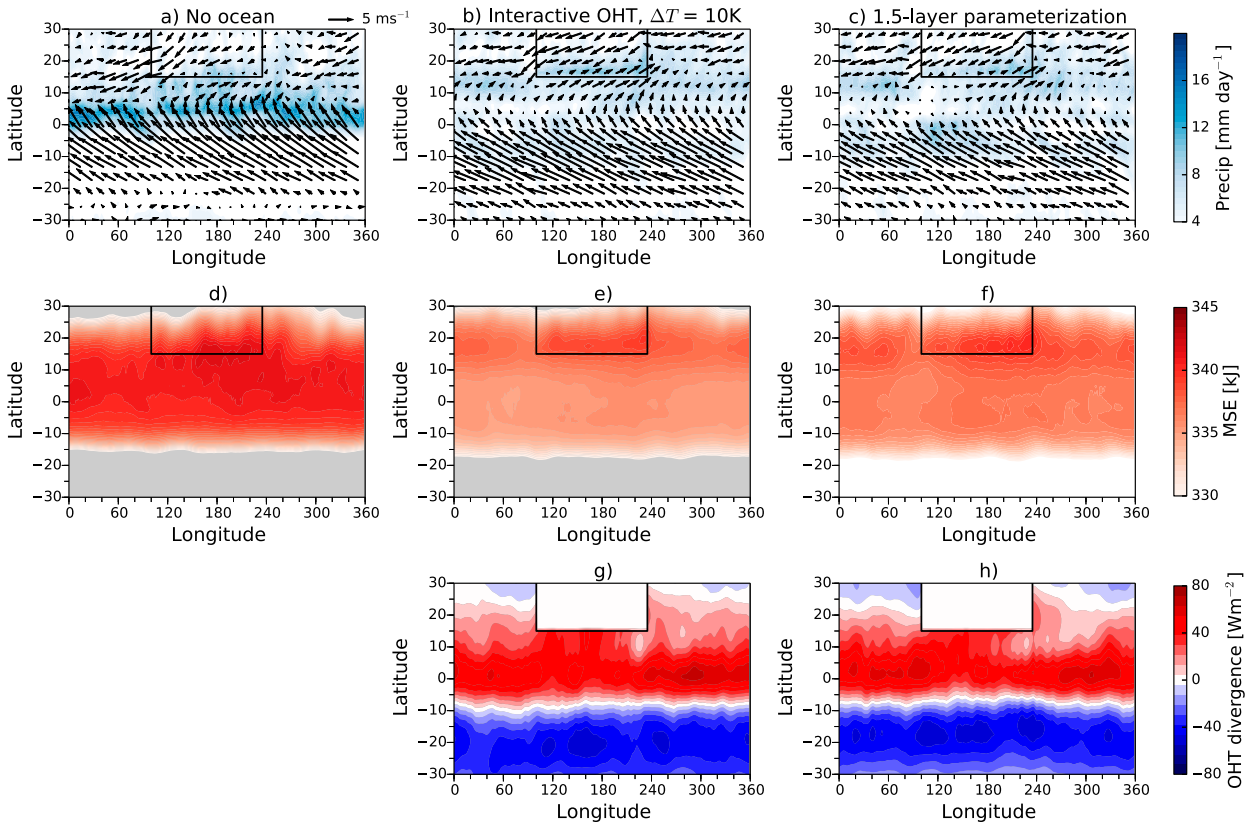

FIG. 3. Summer precipitation (blue contours) and winds at the lowest model level (arrows; same scale in all three panels) for (a) the experiment with no OHT, (b) the experiment with interactive OHT and $\Delta T = 10$ K, and (c) the experiment with the 1.5-layer parameterization. (d)–(f) MSE at the lowest model level from the same experiments. Gray regions have MSE values outside the color bar scale. (g),(h) OHT divergence from the experiments with interactive OHT.

simulations allows the impacts of the OHT on the zonal-mean circulation to be separated out.

3. The relationship between OHT and the model's monsoon

a. *Comparing simulations with and without OHT*

We begin by comparing the monsoons in a simulation without OHT and a simulation with $\Delta T = 10$ K, which is one of our more realistic simulations (see sections 3b and 4). Figure 3 shows the summertime[1] precipitation and surface winds (top panels), the summertime surface moist static energy (middle panels), and the summertime ocean heat flux divergence for the interactive case (bottom right panel). The surface moist static energy is calculated as $c_pT + L_vq_v$, where c_p is the specific heat capacity of dry air, T is the temperature at the lowest model level, L_v is the latent heat of vaporization of liquid water, and q_v is the specific humidity at the lowest model level.

Without OHT, the ITCZ is slightly north of the equator, at about 5°N in the zonal mean, and there is also a weak precipitation maximum just south of the continent (Fig. 3a). The surface MSE is relatively uniform throughout the tropics, with the largest values on the southern edge of the continent. The winds resemble the observations (Fig. 1), being southeasterly up to about 5°N and then swinging around to be southwesterly between 5° and 20°N, although the winds north of 5°N are weak.

In the simulation with $\Delta T = 10$ K there is much clearer evidence of a monsoon, with the highest precipitation over the southern edge of the continent, at about 17°N (Fig. 3b). The winds again resemble the observations, and are stronger between 5° and 20°N than in the no OHT case. The surface MSE is generally smaller than in the simulation without OHT, because the OHT parameterization redistributes heat to the subtropics (see also Clement 2006), and there is a sharper maximum in MSE over the continent, resulting in a larger land–ocean contrast in

[1] "Summer" is defined as the 90 days with the highest insolation over the land and "winter" as the 90 days with the least insolation over the land.

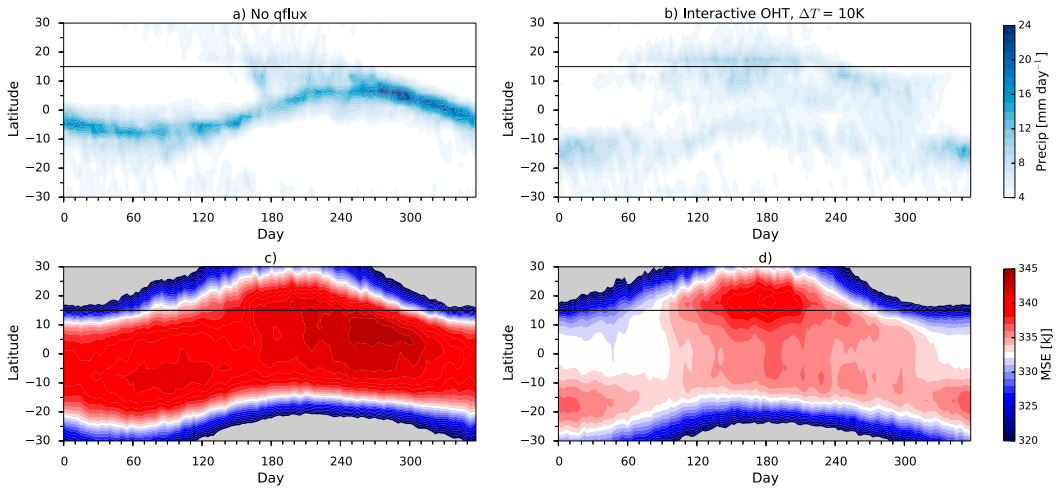

FIG. 4. Seasonal cycles of (a) precipitation and (c) surface MSE, averaged over the land sector (100°–235°E) of the simulation with land but no OHT, calculated from the last seven years of the simulation. (b),(d) As in (a) and (c), respectively, but for the land simulation with interactive OHT and $\Delta T = 10$ K. The horizontal black lines mark the southern edge of the continent.

low-level MSE. Figure 3e shows that the ocean transports heat southward across the equator, as well as from the tropics into the subtropics of the Northern Hemisphere.

Figure 4 compares the seasonal cycles in precipitation (top panels) and surface MSE (bottom panels) in the land sectors of these simulations (100°–235°E), with values averaged over the land sector. Without OHT the maximum precipitation varies smoothly over the course of the year, following the maximum insolation, although there is increased precipitation just south of the land in the late spring and summer months. The MSE shows a similar progression, and the largest MSE is in the summer and early fall because of the larger warming of the land.

The seasonal cycle of precipitation is less regular when OHT is included, and the maximum precipitation is weaker than in the simulation without OHT (Fig. 4b). Both the precipitation and the maximum MSE jump to the warmer hemisphere during the transition seasons so that, as in Clement (2006), the seasonal migration of the ITCZ is larger with OHT. The amplitude of the seasonal cycle in MSE is larger in the Northern Hemisphere than in the Southern Hemisphere, as the highest MSE values are found over the land in the summer months, while the MSE is lower over the land in the winter months than over the equivalent latitudes in the Southern Hemisphere during austral winter. This is discussed further in section 5.

b. Varying ΔT

The effects of varying the strength of the OHT on the surface climate of the model are summarized in Fig. 5. As ΔT is increased the tropical surface temperatures in the land sector cool and the meridional surface temperature gradient is reduced (Fig. 5a). However, the land–ocean surface temperature contrast increases dramatically, going from about 0.2 to 1.5 K as ΔT is increased from 0 to 15 K. The MSE has a similar progression (Fig. 5b), although the profile is smoother, without such a sharp jump across the land–ocean boundary (Fig. 5d). A secondary MSE maximum develops in the southern hemispheres of the experiments with large ΔT. The smoothness of the MSE reflects smoother profiles of near-surface air temperature and specific humidity. We hypothesize that the near-surface air temperature and specific humidity do not track the surface temperature more closely because the air–sea temperature difference must vary in order for the turbulent fluxes of sensible and latent heat to balance the convergence/divergence of OHT. Near-surface advection likely also smooths the MSE profile relative to the sharper land–sea temperature contrast. We also note that, because we set the OHT divergence to zero over the land, the OHT divergence is discontinuous across the land–sea border, potentially exaggerating the land–sea surface temperature contrast.

The ITCZ is close to 5°N in the 0- and 2.5-K simulations, before jumping over the land in the 5-K simulation. This appears to be an intermediate case, as the ITCZs in the 10- and 15-K cases are very similar to each other. The OHT is also similar in these two simulations (Fig. 5e), suggesting that it may saturate for large enough ΔT. Privé and Plumb (2007a) showed that precipitation maxima will occur slightly equatorward of maxima in the surface MSE, where the meridional

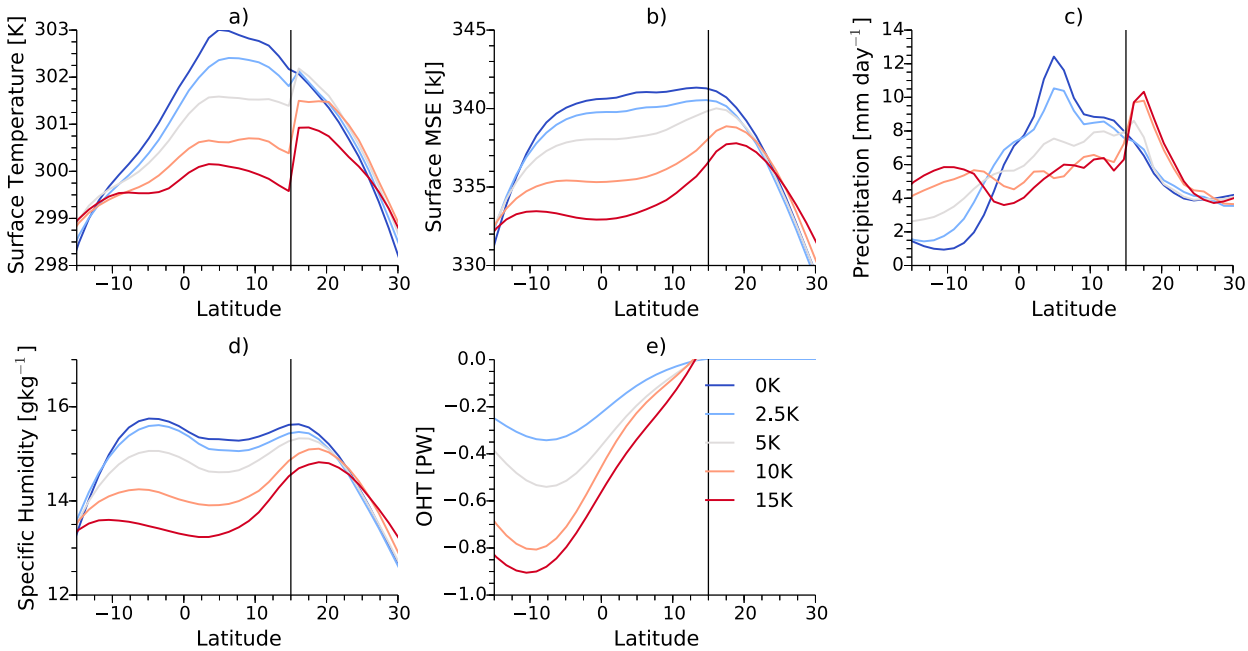

FIG. 5. (a) Summer surface temperatures, averaged from 100° to 235°E, in the simulations with land and with ΔT varied from 0 to 15 K. The vertical line marks the southern boundary of the continent. (b) Average summer surface MSE in these simulations. (c) Average summer precipitation in these simulations. (d) Average summer specific humidity in these simulations. (e) Average summer OHT in these simulations.

gradient in surface MSE (to which the vertical wind shear is proportional) is largest. Although the maximum MSE in the 0- and 2.5-K cases is over the land, there are also MSE maxima near 5°N in these simulations.

Figure 6 plots the zonal winds in these simulations in black contours and the mean meridional circulation (MMC) in the red contours. The MMC is calculated as $(1/g)\int_{p_s}^{p}\overline{v}(p', \phi)dp'$, where an overbar denotes an average over the land sector. (Note that because the average is taken over a limited sector, this circulation does not necessarily conserve mass.) The overturning circulation expands and weakens as ΔT is increased, while the vertical shear in the zonal wind, which is often taken as a proxy for the strength of the monsoonal circulation (Webster and Yang 1992), increases. This is primarily due to a strengthening of the easterlies near the tropopause. For larger ΔT a jump in the near-surface meridional circulation develops just north of the equator because it is difficult for the low-level return flow of the Hadley circulation to cross the equator when the equatorial surface temperature gradient is weak (Pauluis 2004).

The round markers in Fig. 7 quantify these changes by showing the maximum vertical zonal wind shear $[u(850\,\text{hPa}) - u(250\,\text{hPa})]$ between the equator and 20°N as a function of ΔT in Fig. 7a and the minimum (i.e., the most negative) values of the MMC as a function of ΔT in Fig. 7b. The zonal wind shear increases slightly when going from 0 to 2.5 K, then jumps at 5 K and increases roughly linearly as ΔT is increased further. Comparing with Fig. 7c shows that this progression closely tracks the changes in the near-surface MSE gradient. In an angular momentum (AM)-conserving flow the zonal wind shear is proportional to the subcloud MSE gradient (Emanuel 1995); although the flow in these simulations is far from the AM-conserving limit (see below), we believe that this argument is still relevant here.

Conversely, the strength of the MMC decreases roughly linearly from 0 to 10 K and then increases slightly for $\Delta T = 15$ K. The decrease over the first four simulations is expected from the discussion in the introduction: as ΔT is increased the atmosphere has to transport less energy across the equator and so the circulation slows down. A quantitative theory for the compensation between energy transport by the Hadley circulation and OHT is still lacking, however, and in particular requires a better understanding of how the gross moist stability of the tropical atmosphere is controlled (Singh et al. 2017).

Figure 7d shows the minimum absolute vorticity ($f + \overline{\zeta}$, where f is the Coriolis parameter and ζ is the relative vorticity) poleward of 7° during the summer of these simulations. The absolute vorticity vanishes in the upper troposphere of an AM-conserving flow and, although none of the simulations are close to this regime, there is a substantial decrease in the minimum absolute vorticity,

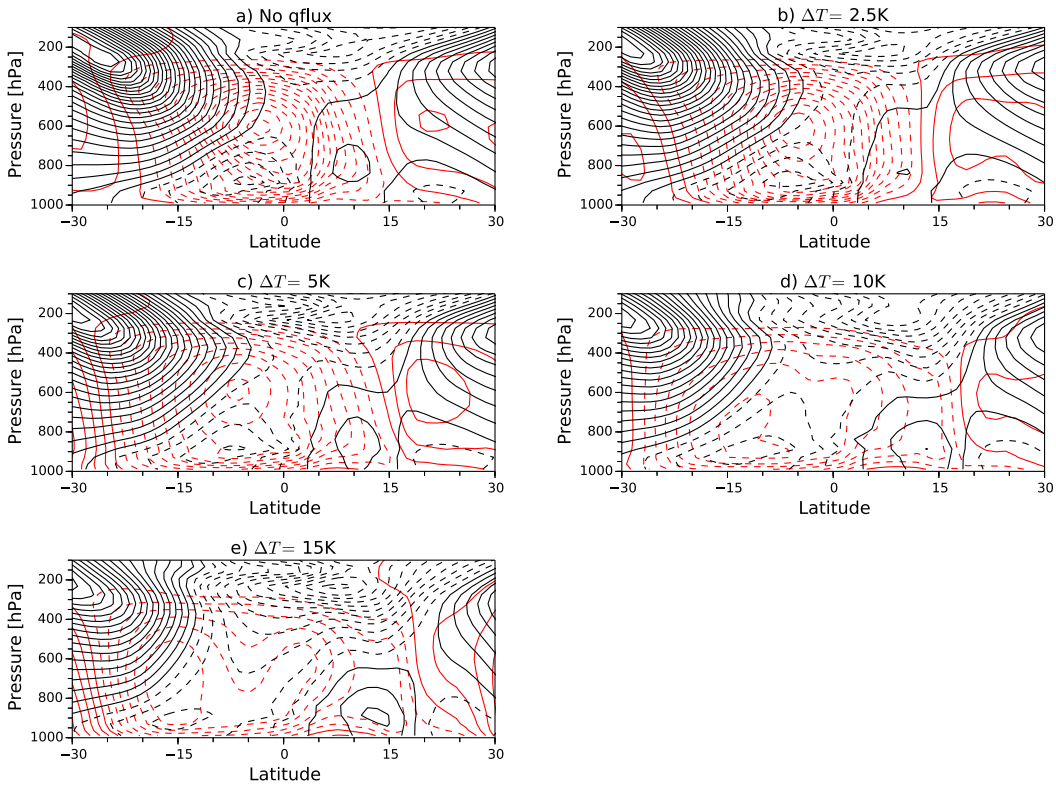

FIG. 6. (a) Summertime MMC (red contours) and zonal winds (black contours) averaged over the land sector (100°–235°E) in the land simulation with $\Delta T = 0$ K. The contour intervals are 2×10^9 kg s^{-1} for the MMC and 2 m s^{-1} for the zonal wind. Dashed red contours denote counterclockwise circulation, and dashed black contours denote negative zonal wind speeds. (b) As in (a), but for the simulation with $\Delta T = 2.5$ K. (c) As in (a), but for the simulation with $\Delta T = 5$ K. (d) As in (a), but for the simulation with $\Delta T = 10$ K. (e) As in (a), but for the simulation with $\Delta T = 15$ K.

from about 0.55×10^{-5} to 0.41×10^{-5} s^{-1} when going from $\Delta T = 10$ K to $\Delta T = 15$ K. This step toward an AM-conserving flow is caused by the increased vertical wind shear, as the stronger upper-level easterlies shield the tropical circulation from baroclinic eddies originating at midlatitudes (Bordoni and Schneider 2008). Since these eddies act as a drag on the mean flow, increased shielding may explain why the MMC strengthens in the $\Delta T = 15$ K case (Walker and Schneider 2006).

In summary, increasing ΔT both strengthens the monsoonal circulation by increasing the land–sea contrast and damps the monsoon because less heat needs to be carried across the equator by the atmosphere.

c. *Specifying the OHT*

The effects of the OHT on the monsoon come partly from the seasonal variations in the OHT and partly from the effects of the annual-mean OHT. Our second set of simulations separate these out, as the OHT is fixed at the annual-mean profiles from the interactive experiments. The crosses in the top panels of Fig. 7 show that this increases the maximum zonal-wind shear and also the MMC. The MSE gradient also increases (Fig. 7c), while the minimum absolute vorticity decreases rapidly, so that the flow is approximately AM-conserving for $\Delta T = 10$ K and above (Fig. 7d). While this transition to an AM-conserving regime will strengthen the flow somewhat, Fig. 7e shows that in fact the MMC scales linearly with the OHT at the equator, so that the energetic requirements on the Hadley circulation are the dominant control on its strength.

More insight into the effects of specifying the OHT on the monsoon comes from the left panels of Fig. 8, which show the summer climate in the case with the OHT from the $\Delta T = 10$ K case. The monsoon is stronger than in the corresponding case with interactive OHT, with stronger winds and precipitation, as well as a larger land–sea MSE contrast. The shape of the winds means in particular that the monsoon is strongest in the southeast corner of the continent. The reason for this stronger monsoon can be seen by comparing Fig. 8e, which shows the OHT divergence in this simulation, with Fig. 3e. The annual-mean OHT is still southward in the land sector, but the ocean now converges heat at the latitudes of the

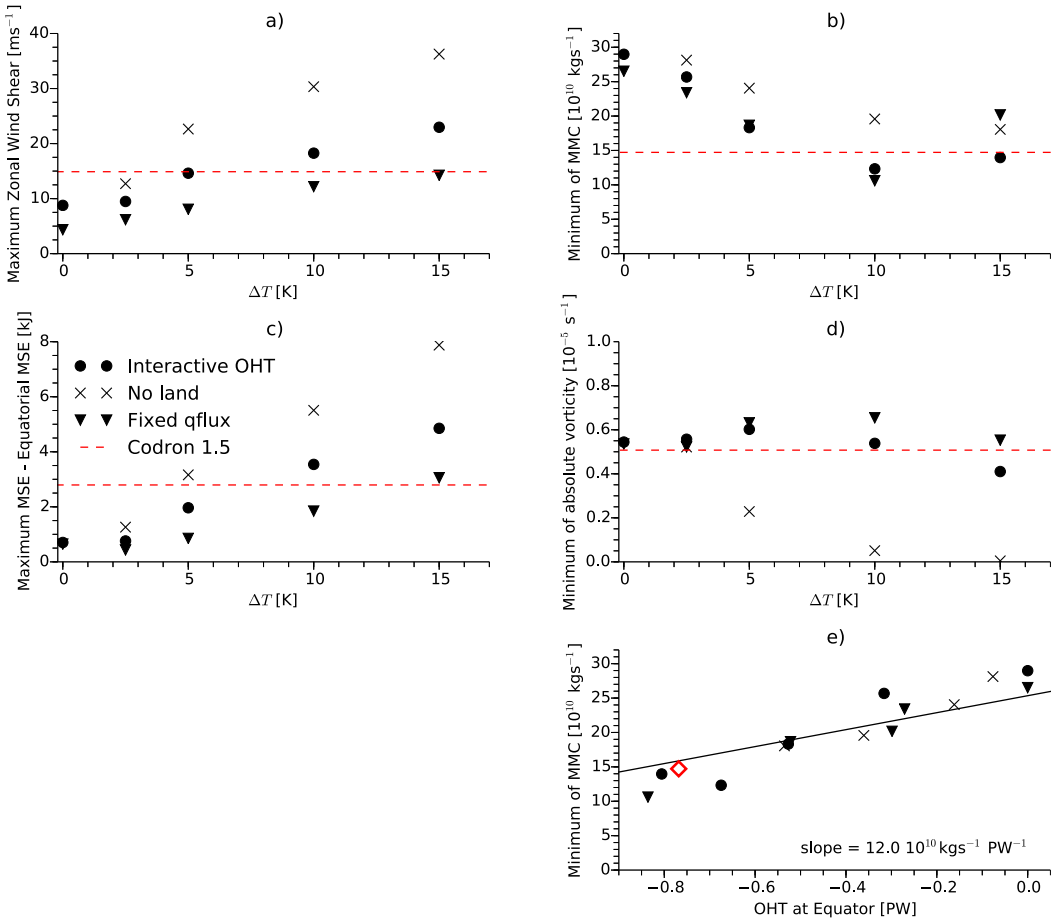

FIG. 7. (a) Maximum of [u(850 hPa) − u(250 hPa)], averaged over the land sector (100°–235°E), between the equator and 20°N during the summer months for the simulations with land and interactive OHT (circles), the simulations with interactive OHT and no land (crosses) and with land and OHT fixed at its annual-mean values (triangles). (b) Minimum of the summertime MMC for the same simulations. (c) Difference between maximum summer MSE and equatorial MSE at the equator for the same simulations. (d) Minimum absolute vorticity poleward of 7°N during the summer of the same simulations. (e) Minimum of the summertime MMC for the same simulations as a function of the equatorial OHT in the land sector. The line shows a linear least squares fit. In (a)–(d) the dashed red lines show the results from the experiment with the Codron (2012) 1.5-layer parameterization, and the red diamond in (e) shows the minimum summertime MMC and the equatorial OHT for the experiment with the Codron parameterization.

south coast of the continent (15°–20°), rather than diverging heat as it was in the interactive case. This warms the waters on either side of the continent, so that the continent is not cooled as much by zonal breezes as it was in the interactive case. This is reminiscent of how Privé and Plumb (2007b) found that adding walls to their continent strengthened the monsoon by insulating it from zonal sea breezes (see the introduction).

4. Comparison with more realistic models

The above results give an indication of how OHT might affect monsoon circulations; however, the idealized nature of our model puts into question the relevance of our results for the real atmosphere. As a first way of assessing this, the dashed red lines in Fig. 7 show values from the simulation with the 1.5-layer parameterization. These generally lie between the ΔT = 5 K and ΔT = 10 K simulations, with the vertical wind shear closer to the 5-K case and the MMC closer to the 10-K case. Comparing the middle column with the right column of Fig. 3 also demonstrates the similarities between the 1.5-layer simulation and the ΔT = 10 K case. So even with ΔT allowed to vary with latitude in a realistic manner, OHT has a major impact on the monsoon circulation in this model.

Next, we investigate the seasonal cycles of SSTs equatorward of the land and of the ocean heat budget

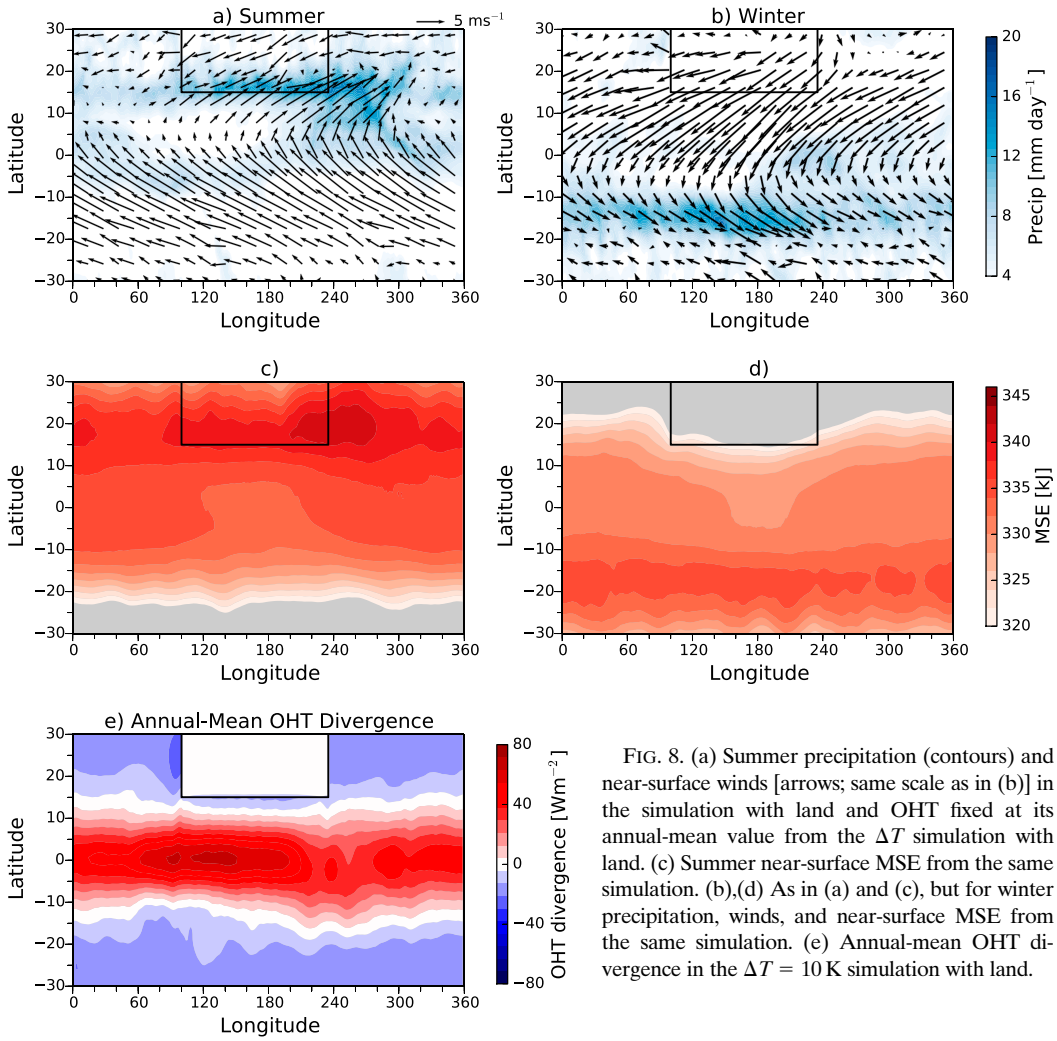

FIG. 8. (a) Summer precipitation (contours) and near-surface winds [arrows; same scale as in (b)] in the simulation with land and OHT fixed at its annual-mean value from the ΔT simulation with land. (c) Summer near-surface MSE from the same simulation. (b),(d) As in (a) and (c), but for winter precipitation, winds, and near-surface MSE from the same simulation. (e) Annual-mean OHT divergence in the $\Delta T = 10$ K simulation with land.

in our simulations. As stated in section 2b, a drawback of the interactive OHT parameterization is that the mixed layer depth (MLD) is kept fixed: in the real ocean changes in OHT do not necessarily lead to changes in SSTs, because the MLD may also deepen or shoal. Moreover, the circulation and temperature in the thermocline take time to adjust to different surface conditions, whereas this adjustment is instantaneous in both our simple parameterization and the 1.5-layer parameterization. These two deficiencies mean that our model misses any potential phase difference between changing surface winds and OHT-induced SST variations.

The heat budget for a volume of ocean water is

$$Q_S(t) = Q_O(t) + Q_F(t), \tag{9}$$

where Q_S is the change in heat stored in the volume:

$$Q_S(t) = a^2 \rho c_{p,0} \int_{\mathrm{MLD}}^{0} \int_{\phi_1}^{\phi_2} \int_{\lambda_1}^{\lambda_2} \frac{dT}{dt} \cos\phi \, d\lambda \, d\phi \, dz, \tag{10}$$

where ρ is the density of seawater and T is the depth-averaged temperature of the mixed layer. Here, Q_O is the OHT (q_O) integrated around the lateral boundaries of the volume, as well as heat fluxed through the bottom of the mixed layer (which we ignore), and Q_F is the surface heat flux into the water:

$$Q_F(t) = a^2 \int_{\phi_1}^{\phi_2} \int_{\lambda_1}^{\lambda_2} (Q_{\mathrm{SW}} + Q_{\mathrm{LW}} + Q_{\mathrm{LH}} + Q_{\mathrm{SH}}) \cos\phi \, d\lambda \, d\phi, \tag{11}$$

where Q_{SW} is the incoming solar radiation at the surface, Q_{LW} is the outgoing longwave radiation at the surface, Q_{LH} is the surface latent heat flux and Q_{SH} is the surface sensible heat flux. Note that if Q_F is fixed then

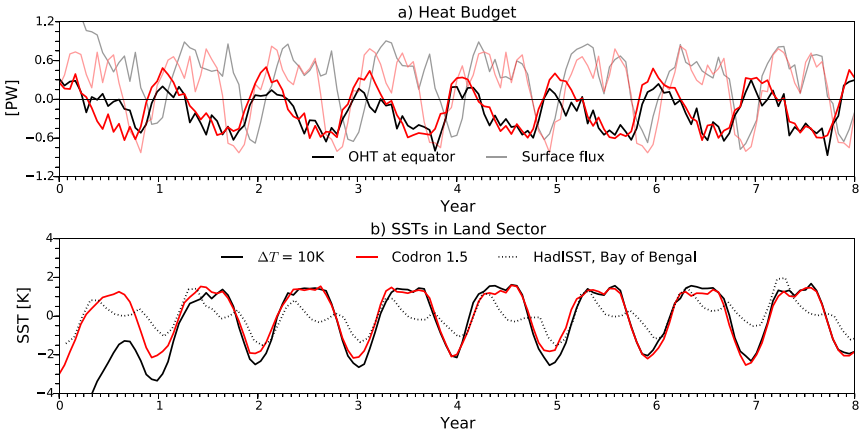

FIG. 9. (a) Ocean heat transport across the equator, integrated from 100° to 235°E (thick lines) and net surface flux integrated over the region from 100° to 235°E and from 0° to 15°N (thin lines), from the land simulation with $\Delta T = 10$ K (black lines) and with the 1.5-layer parameterization (red lines). The heat transport is positive when it is northward. (b) SSTs averaged over the region 100°–235°E, 0°–15°N from the simulation with $\Delta T = 10$ K (solid black line) and the simulation with the 1.5-layer parameterization (red line) and SSTs averaged over the Bay of Bengal (80°–95°E, 0°–15°N) for the period 2008–16, taken from the HadISST dataset (dotted black line).

changes in Q_O can be compensated either by changes in T or by changes in the MLD and so, since the MLD is fixed in our model, changes in Q_O can only be compensated by changes in T.

Figure 9a shows the heat budget for the ocean south of the continent (100°–235°E, 0°–15°N) in the simulation with land and $\Delta T = 10$ K in black, and for the 1.5-layer simulation in red. In both simulations, the ocean carries heat north across the equator in winter and south in summer, while it is warmed by the surface fluxes in summer and cooled in the winter. The largest surface fluxes are in the spring and in the fall because the strong monsoon winds in the summer lead to enhanced evaporative cooling over the ocean. These terms produce a seasonal cycle in the SSTs of ~4 K in the $\Delta T = 10$ K case (solid line in Fig. 9b) and ~3 K in the 1.5-layer simulation (dotted red line), with the warmest SSTs in both cases coming in the fall when the OHT and the monsoonal winds are weaker.

These results agree qualitatively with previous studies of the heat budget of the NIO, although there are some notable differences. Comparing with Fig. 3 of Chirokova and Webster (2006), the seasonal cycles of the OHT and of the surface fluxes in our simulations are similar to their modeled NIO, except that the OHT is generally larger than the surface fluxes in their simulations whereas the reverse is the case in our simulations [see also Fig. 21 of Lee and Marotzke (1998)], although we note that because of our idealized setup we are not averaging over the same geometries. The other major difference is that Chirokova and Webster (2006) and Lee and Marotzke (1998) both find that Q_F is almost zero during the summer and early fall, because increased cloudiness reduces the solar radiation absorbed by the surface (as a reminder, there are no clouds in our model) and because of stronger evaporative cooling than in our simulations, caused by stronger monsoonal winds. The large reduction in Q_F in the summer means that the warmest SSTs in the NIO are actually in April and May (dashed black line in Fig. 9b), rather than in the fall.

Babu et al. (2004) showed that the MLD in the NIO is shallowest in February and March, which contributes to the warm SSTs in the spring, and then deepens over the course of the summer due to mixing caused by the monsoonal winds. The mixed layer shoals rapidly again in the fall at the end of the monsoon season and then deepens in the winter months. The gradual deepening of the mixed layer during the summer will damp the cooling of the NIO SSTs by OHT during the summer months, but on the whole we believe that our model underestimates the cooling of SSTs by OHT, and the amplitude of the seasonal cycle of SSTs in the NIO is smaller than in our model (Fig. 9b). Although there are differences between the heat budgets in our model and in the more realistic models of Lee and Marotzke (1998) and Chirokova and Webster (2006) due to the fixed mixed layer depth and the lack of clouds in our model, we believe that our model qualitatively captures the impact of OHT on SSTs equatorward of subtropical continents, and that the effects of any phase lag are minor.

5. Zonal-mean effects

The behavior discussed in section 3 comes from the monsoon generated over the land, but also from the

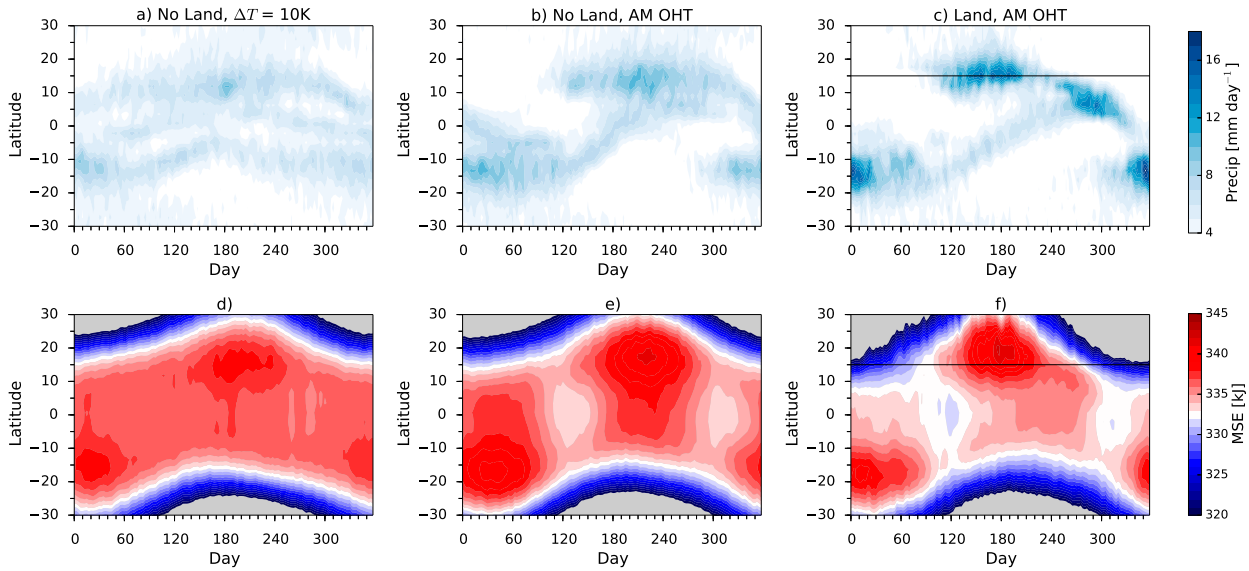

FIG. 10. Seasonal cycle of (a) zonal-mean precipitation and (d) the meridional gradient of surface MSE, calculated over the last 7 years of the simulation with no land and $\Delta T = 10$ K. (b),(e) As in (a) and (d), but for the simulation without land and with OHT fixed at its annual-mean value from the $\Delta T = 10$ K simulation. (c),(f) As in (a) and (d), but for the simulation with land and with OHT fixed at its annual-mean value from the $\Delta T = 10$ K simulation.

zonal-mean effects of the interactive OHT. We use our third set of experiments—with interactive OHT but no land—to investigate how the interactive OHT affects the zonal-mean circulation of the model.

The triangles in Fig. 7a show that excluding the land reduces the vertical zonal wind shear by roughly half, although this still increases as ΔT is increased and the MSE gradient also strengthens (Fig. 7b). So, even without the land the southward energy transport by the ocean still produces a monsoon-like circulation. The MMC is very similar with and without land (Fig. 7b), as it is mostly determined by the OHT (section 3c).

These experiments, together with the fixed OHT experiments, can also be used to understand the seasonal cycles in Fig. 4. In the simulation without land and with $\Delta T = 10$ K there are actually three maxima in the precipitation (Fig. 10a), one close to the equator and one farther poleward in each hemisphere, with all three shifting gradually over the course of the year. A double-ITCZ structure is expected because the OHT and the heat transport by the atmosphere result in the net energy input to the deep tropics being negative (Clement 2006; Bischoff and Schneider 2016), while the peak at the equator is caused by rising motion as the meridional circulation jumps over the equator (not shown).

The seasonal cycle in the fixed OHT experiment resembles the seasonal cycle in the simulation with interactive OHT, but with the features exaggerated (Figs. 10c,f). In the winter there is very little precipitation in the Northern Hemisphere and a strong maximum in precipitation at about 15°S. A strong maximum appears in the Northern Hemisphere over the land in the spring, while the maximum in the Southern Hemisphere weakens and gradually shifts to the north, joining the strong peak over the land in the late summer. During the fall the maximum slowly migrates southward, before jumping farther south once winter sets in.

These jumps are primarily caused by strong surface winds blowing south off the continent in the winter (Fig. 8b). Because the continent is very cold in the winter, these winds cool the oceans to the south of the continent, creating a strong meridional MSE gradient compared to the warmer waters of the Southern Hemisphere (Fig. 8d; note that the MSE near the equator is colder than in the summer). These winds die down in the spring as the land—as well as the oceans to either side of it—warms up, rapidly reducing the MSE gradient and causing a strong MSE and precipitation maximum to develop over the continent. At the same time, the precipitation maximum in the south migrates northward, following the peak insolation, until it merges with the maximum over the land. In the fall the land cools and the MSE maximum gradually migrates southward until the strong winds pick up again, rapidly cooling the ocean and causing the jump to the strong southern precipitation maximum during winter.

We have performed an additional experiment without land and with the OHT fixed at its annual-mean value from the no-land $\Delta T = 10$ K experiment. This is similar to the fixed OHT with land, although the precipitation

maxima are weaker (Fig. 10b). The MSE is smallest in the transition months (Fig. 10e), when it has a minimum near the equator because the atmosphere and ocean transport heat to higher latitudes, resulting in a double ITCZ. In the summer and winter, the atmosphere transfers heat into the tropics, so that they gain energy in the net (not shown) and there is a single ITCZ.

Together, these can explain the features seen in Fig. 4. The jumps in the precipitation maximum and in the MSE maximum come about because of the rapid warming and cooling of the continent, but at the same time the interactive OHT promotes a double ITCZ, as there is net energy transport out of the deep tropics.

6. Conclusions

In this study we have investigated the monsoon in an idealized model consisting of the widely used gray-radiation atmospheric GCM, coupled to an idealized parameterization of ocean heat transport by the subtropical cells. The OHT parameterization includes a parameter ΔT that can be used to vary the strength of the OHT, allowing us to systematically investigate the impact of OHT on the monsoon in this model.

Without OHT the monsoon in our model is weak, because the land surface is not protected from cold winds coming either from farther north or from the east and west of the land [see also Chou et al. (2001) and Privé and Plumb (2007b)]. However, by increasing ΔT sufficiently we are able to create a reasonable monsoon circulation because the waters south of the land cool during the summer, creating a strong meridional MSE gradient. This includes increases in the vertical wind shear as ΔT is increased and in the precipitation over land, though the MMC weakens. The shear strengthens because the meridional MSE gradient increases, while the MMC weakens because the increased OHT means that the atmosphere is required to transport less heat across the equator (Clement 2006; Singh et al. 2017). For $\Delta T = 15\,\mathrm{K}$ the vertical shear is strong enough to start pushing the flow toward an angular momentum–conserving regime. Fixing the OHT at its annual-mean value results in the OHT warming the waters zonally adjacent to the land, rather than cooling them, as in the case with interactive OHT, but the waters south of the land are still cooled as there is southward OHT in the land sector (Fig. 8e). This increases the MSE gradient compared to the interactive case, resulting in a stronger monsoon circulation, which causes the flow in the simulations with $\Delta T = 10\,\mathrm{K}$ and above to be in an AM-conserving regime. Comparisons with a simulation that uses the 1.5-layer parameterization of Codron (2012) and with the results of Chirokova and Webster (2006) and Lee and Marotzke (1998) suggest that our most realistic cases are the $\Delta T = 5\,\mathrm{K}$ and $\Delta T = 10\,\mathrm{K}$ simulations and that, if anything, our model underestimates the effects of OHT on SSTs south of subtropical continents.

Combining the original experiments with the fixed OHT experiments and the experiments without land shows that the changes in the MMC are largely due to changes in the OHT, with the MMC weakening as the OHT increased. By contrast, the presence of land and/or of a transition to an AM-conserving regime has minor impacts on the MMC, except insofar as they affect the OHT. Finally, the seasonal cycle of precipitation in the interactive OHT simulations exhibits jumps, as strong precipitation suddenly appears over the continent in the summer and in the Southern Hemisphere during winter. These jumps are even clearer in the simulations with fixed OHT, and are caused by strong winds blowing off the continent during the winter months, which cool the waters south of the continent and set up a strong MSE maximum in the Southern Hemisphere. When the land warms up sufficiently these winds stop and the waters north of the equator warm up quickly, while an MSE maximum develops over the land. When the land starts to cool in the fall the MSE maximum at first gradually shifts southward, until the strong winds reappear and the maximum MSE jumps southward. The jumps are clearer in the simulations without the interactive OHT because removing the link between OHT and the surface winds reduces the variability of the precipitation and also makes the model less likely to have a double ITCZ.

These results have been obtained with an idealized model, but demonstrate the substantial impact OHT can have on the monsoonal circulation, both through the zonal-mean effect of the atmosphere needing to transport less heat across the equator and through the local effect of creating a stronger meridional MSE gradient. Work with more comprehensive models, which include clouds and realistic topography, is required to further assess the impact these effects have on the South Asian monsoon, which is the original motivation for our study. Simulations with more realistic representations of ocean dynamics will also be required to assess whether any of the effects seen here are distorted by our highly idealized model setup. Finally, as has been noted in several previous studies, a theory for the compensation between the ocean and the atmosphere is required in order to quantitatively predict how the overturning circulation is affected by the increased OHT, particularly a theory for how the gross moist stability of the tropical atmosphere is affected.

The Indian subcontinent seems to be ideally situated to develop a strong monsoon, being insulated from cold winds blowing down from Eurasia by the Himalayas to

the north, while to the south the northern Indian Ocean transports heat southward, cooling the SSTs off the coast of India and further enhancing the meridional MSE gradient. Previous studies have mostly focused on the effects of the Himalayas and the Tibetan Plateau on the monsoon, and have used either prescribed SSTs (e.g., Boos and Kuang 2010; Ma et al. 2014) or slab oceans with Q fluxes added to ensure the slab's SSTs closely match the observed climatological-mean SSTs (Park et al. 2012). At the same time, in simulations with coupled models in which Asian orography is flattened the South Asian monsoon is weakened, but not eliminated, and these simulations give an indication of the influence of OHT in the northern Indian Ocean on the monsoon (Naiman et al. 2017; Baldwin et al. 2019). Putting these different modeling approaches together to fully characterize the influences of both the Himalayas and Tibet and of OHT in the northern Indian Ocean will be required for a complete picture of the South Asian monsoon.

Acknowledgments. We thank Peter Webster and Tim Cronin for helpful discussions, and three anonymous reviewers, whose comments substantially improved the manuscript. Nicholas Lutsko was partly supported by NSF Grant AGS-1623218, "Collaborative Research: Using a Hierarchy of Models to Constrain the Temperature Dependence of Climate Sensitivity," and Brian Green was partly supported by a grant from NOAA.

REFERENCES

Babu, K. N., R. Sharma, N. Agarwal, V. K. Agarwal, and R. A. Weller, 2004: Study of the mixed layer depth variations within the north Indian Ocean using a 1-D model. *J. Geophys. Res.*, **109**, C08016, https://doi.org/10.1029/2003JC002024.

Baldwin, J. W., G. A. Vecchi, and S. Bordoni, 2019: The direct and ocean-mediated influence of Asian topography on tropical precipitation and cyclones. *Climate Dyn.*, https://doi.org/10.1007/s00382-019-04615-5.

Bischoff, T., and T. Schneider, 2016: The equatorial energy balance, ITCZ position, and double-ITCZ bifurcations. *J. Climate*, **29**, 2997–3013, https://doi.org/10.1175/JCLI-D-15-0328.1.

Boos, W. R., and Z. Kuang, 2010: Dominant control of the South Asian monsoon by orographic insulation versus plateau heating. *Nature*, **463**, 218–222, https://doi.org/10.1038/nature08707.

Bordoni, S., and T. Schneider, 2008: Monsoons as eddy-mediated regime transitions of the tropical overturning circulation. *Nat. Geosci.*, **1**, 515–519, https://doi.org/10.1038/ngeo248.

Chirokova, G., and P. J. Webster, 2006: Interannual variability of Indian Ocean heat transport. *J. Climate*, **19**, 1013–1031, https://doi.org/10.1175/JCLI3676.1.

Chou, C., J. D. Neelin, and H. Su, 2001: Ocean–atmosphere–land feedbacks in an idealized monsoon. *Quart. J. Roy. Meteor. Soc.*, **127**, 1869–1891, https://doi.org/10.1002/qj.49712757602.

Clement, A. C., 2006: The role of the ocean in the seasonal cycle of the Hadley circulation. *J. Atmos. Sci.*, **63**, 3351–3365, https://doi.org/10.1175/JAS3811.1.

Codron, F., 2012: Ekman heat transport for slab oceans. *Climate Dyn.*, **38**, 379–389, https://doi.org/10.1007/s00382-011-1031-3.

Czaja, A., and J. Marshall, 2006: The partitioning of poleward heat transport between the atmosphere and ocean. *J. Atmos. Sci.*, **63**, 1498–1511, https://doi.org/10.1175/JAS3695.1.

Donohoe, A., D. M. W. Frierson, and D. S. Battisti, 2014: The effect of ocean mixed layer depth on climate in slab ocean aquaplanet experiments. *Climate Dyn.*, **43**, 1041–1055, https://doi.org/10.1007/s00382-013-1843-4.

Emanuel, K. A., 1995: On thermally direct circulations in moist atmospheres. *J. Atmos. Sci.*, **52**, 1529–1534, https://doi.org/10.1175/1520-0469(1995)052<1529:OTDCIM>2.0.CO;2.

Frierson, D. M. W., 2007: The dynamics of idealized convection schemes and their effect on the zonally averaged tropical circulation. *J. Atmos. Sci.*, **64**, 1959–1976, https://doi.org/10.1175/JAS3935.1.

——, I. M. Held, and P. Zurita-Gotor, 2006: A gray-radiation aquaplanet moist GCM. Part I: Static stability and eddy scales. *J. Atmos. Sci.*, **63**, 2548–2566, https://doi.org/10.1175/JAS3753.1.

Geen, R., F. H. Lambert, and G. K. Vallis, 2018: Regime change behavior during Asian monsoon onset. *J. Climate*, **31**, 3327–3348, https://doi.org/10.1175/JCLI-D-17-0118.1.

Green, B., and J. Marshall, 2017: Coupling of trade winds with ocean circulation damps ITCZ shift. *J. Climate*, **30**, 4395–4411, https://doi.org/10.1175/JCLI-D-16-0818.1.

Hartmann, D. L., 2016: *Global Physical Climatology*. 2nd ed. Elsevier, 498 pp.

Held, I. M., 2001: The partitioning of the poleward energy transport between the tropical ocean and atmosphere. *J. Atmos. Sci.*, **58**, 943–948, https://doi.org/10.1175/1520-0469(2001)058<0943:TPOTPE>2.0.CO;2.

Hilgenbrink, C. C., and D. L. Hartmann, 2018: The response of Hadley circulation extent to an idealized representation of poleward ocean heat transport in an aquaplanet GCM. *J. Climate*, **31**, 9753–9770, https://doi.org/10.1175/JCLI-D-18-0324.1.

Klinger, B. A., and J. Marotzke, 2000: Meridional heat transport by the subtropical cell. *J. Phys. Oceanogr.*, **30**, 696–705, https://doi.org/10.1175/1520-0485(2000)030<0696:MHTBTS>2.0.CO;2.

Lee, T., and J. Marotzke, 1998: Seasonal cycles of meridional overturning and heat transport of the Indian Ocean. *J. Phys. Oceanogr.*, **28**, 923–943, https://doi.org/10.1175/1520-0485(1998)028<0923:SCOMOA>2.0.CO;2.

Levine, X. J., and T. Schneider, 2011: Response of the Hadley circulation to climate change in an aquaplanet GCM coupled to a simple representation of ocean heat transport. *J. Atmos. Sci.*, **68**, 769–783, https://doi.org/10.1175/2010JAS3553.1.

Levitus, S., 1987: Meridional Ekman heat fluxes for the world ocean and individual ocean basins. *J. Phys. Oceanogr.*, **17**, 1484–1492, https://doi.org/10.1175/1520-0485(1987)017<1484:MEHFFT>2.0.CO;2.

Loschnigg, J., and P. J. Webster, 2000: A coupled ocean–atmosphere system of SST modulation for the Indian Ocean. *J. Climate*, **13**, 3342–3360, https://doi.org/10.1175/1520-0442(2000)013<3342:ACOASO>2.0.CO;2.

Ma, D., W. R. Boos, and Z. Kuang, 2014: Effects of orography and surface heat fluxes on the South Asian summer monsoon. *J. Climate*, **27**, 6647–6659, https://doi.org/10.1175/JCLI-D-14-00138.1.

McCreary, J. P., P. K. Kundu, and R. L. Molinari, 1993: A numerical investigation of the dynamics, thermodynamics and mixed layer processes in the Indian Ocean. *Prog. Oceanogr.*, **31**, 181–244, https://doi.org/10.1016/0079-6611(93)90002-U.

Naiman, Z., P. J. Goodman, J. P. Krasting, S. L. Malyshev, J. L. Russell, R. J. Stougger, and A. T. Wittenberg, 2017: Impact of mountains on tropical circulation in two Earth system models. *J. Climate*, **30**, 4149–4163, https://doi.org/10.1175/JCLI-D-16-0512.1.

O'Gorman, P. A., and T. Schneider, 2008: The hydrological cycle over a wide range of climates simulated with an idealized GCM. *J. Climate*, **21**, 3815–3832, https://doi.org/10.1175/2007JCLI2065.1.

Park, H.-S., J. C. H. Chiang, and S. Bordoni, 2012: The mechanical impact of the Tibetan Plateau on the seasonal evolution of the South Asian monsoon. *J. Climate*, **25**, 2394–2407, https://doi.org/10.1175/JCLI-D-11-00281.1.

Pauluis, O., 2004: Boundary layer dynamics and cross-equatorial Hadley circulation. *J. Atmos. Sci.*, **61**, 1161–1173, https://doi.org/10.1175/1520-0469(2004)061<1161:BLDACH>2.0.CO;2.

Plumb, R. A., and A. Y. Hou, 1992: The response of a zonally symmetric atmosphere to subtropical thermal forcing: Threshold behavior. *J. Atmos. Sci.*, **49**, 1790–1799, https://doi.org/10.1175/1520-0469(1992)049<1790:TROAZS>2.0.CO;2.

Privé, N. C., and R. A. Plumb, 2007a: Monsoon dynamics with interactive forcing. Part I: Axisymmetric studies. *J. Atmos. Sci.*, **64**, 1417–1430, https://doi.org/10.1175/JAS3916.1.

——, and ——, 2007b: Monsoon dynamics with interactive forcing. Part II: Impact of eddies and asymmetric geometries. *J. Atmos. Sci.*, **64**, 1431–1442, https://doi.org/10.1175/JAS3917.1.

Schneider, T., 2017: Feedback of atmosphere–ocean coupling on shifts of the intertropical convergence zone. *Geophys. Res. Lett.*, **44**, 11 644–11 653, https://doi.org/10.1002/2017GL075817.

Schott, F. A., S.-P. Xie, and J. P. McCreary, 2009: Indian Ocean circulation and climate variability. *Rev. Geophys.*, **47**, RG1002, https://doi.org/10.1029/2007RG000245.

Singh, M. S., Z. Kuang, and Y. Tian, 2017: Eddy influences on the strength of the Hadley circulation: Dynamic and thermodynamic perspectives. *J. Atmos. Sci.*, **74**, 467–486, https://doi.org/10.1175/JAS-D-16-0238.1.

Vecchi, G. A., and D. E. Harrison, 2002: Monsoon breaks and subseasonal sea surface temperature variability in the Bay of Bengal. *J. Climate*, **15**, 1485–1493, https://doi.org/10.1175/1520-0442(2002)015<1485:MBASSS>2.0.CO;2.

Walker, C. C., and T. Schneider, 2006: Eddy influences on Hadley circulations: Simulations with an idealized GCM. *J. Atmos. Sci.*, **63**, 3333–3350, https://doi.org/10.1175/JAS3821.1.

Webster, P. J., and S. Yang, 1992: Monsoon and ENSO: Selectively interactive systems. *Quart. J. Roy. Meteor. Soc.*, **118**, 877–926, https://doi.org/10.1002/qj.49711850705.

——, C. Clark, G. Cherikova, J. Fasulla, W. Han, J. Loschnigg, and K. Sahami, 2002: The monsoon as a self-regulating coupled ocean–atmosphere system. *Int. Geophys.*, **83**, 198–219, https://doi.org/10.1016/S0074-6142(02)80168-1.

Zhai, J., and W. Boos, 2015: Regime transitions of cross-equatorial Hadley circulations with zonally asymmetric thermal forcings. *J. Atmos. Sci.*, **72**, 3800–3818, https://doi.org/10.1175/JAS-D-15-0025.1.